Calculating Orbits of the Dwarfs and High Velocity Stars of Milky Way

Mentee: Upendra Sen Chakma
BSc in Physics, Physics Discipline, Khulna University
Mentor: Istiak Hossain Akib
PhD candidate, Observatoire de Paris, France

ICTP PWF: Physics For Bangladesh Summer Internship Program
(Online)

November 5, 2025

Declaration

I, **Upendra Sen Chakma**, hereby declare that this internship report titled *"Calculating Orbits of the Dwarfs and High Velocity Stars of Milky Way"* is an original work done by me under the supervision of **Istiak Hossain Akib** (PhD Candidate, Observatoire de Paris, France) as part of the ICTP PWF: Physics For Bangladesh Summer Internship Program.

Acknowledgment

I express my profound gratitude to my mentor, **Istiak Hossain Akib**, PhD Candidate at the Observatoire de Paris, for his exceptional guidance, constant support, and invaluable feedback throughout this internship. His expertise in computational astrophysics and orbital mechanics has been instrumental in shaping this research.

I am deeply grateful to the **International Centre for Theoretical Physics (ICTP)** for providing this exceptional opportunity through the ICTP PWF: Physics For Bangladesh Program. The program has been transformative for my professional development and research capabilities. I thank the **Gaia Mission** for providing publicly accessible astronomical data that forms the foundation of this research. I also acknowledge the developers of **Galpy**, **Plotly**, **Astropy**, and other open-source astronomical software packages that made this computational analysis possible.

Contents

Chapter 1

Abstract

This report presents a comprehensive computational investigation into the orbital dynamics of the Large Magellanic Cloud (LMC) and Small Magellanic Cloud (SMC) as they interact with the Milky Way. Utilizing the Galpy Python library and both MWPotential2014 and MWPotJ23 Galactic models, the study integrates recent data from Gaia and Hubble Space Telescope to initialize precise orbital parameters for the LMC and SMC. Monte Carlo method with uncertainty propagation were conducted across 100 realizations for each galaxy, mapping their trajectories and quantifying the probabilities of close encounters over a 3 Gyr timescale. Core results reveal the timing, frequency, and separation scales of LMC-SMC interactions, and demonstrate how these encounters shape the formation of tidal features such as the Magellanic Stream and Bridge. In addition, this work undertakes the first orbital analysis of hypervelocity stars (HVS) relative to the Milky Way, LMC, and SMC, showing that phase-space clustering of HVS directly reflects recent galactic interactions and tidal ejections. Heatmap visualizations, probability calculations, and detailed kinematic studies provide new evidence that the Magellanic Clouds not only perturb the Galactic halo but also contribute to its population of high-velocity stars. These findings refine current models of satellite evolution, highlight the dynamical importance of the Magellanic System, and offer constraints on the mass profile and dark matter distribution of the Milky Way establishing an integrated view that connects dwarf galaxy interactions, stellar debris formation, and the future structure of our Galaxy.

Chapter 2

Introduction

The Large Magellanic Cloud (LMC) and Small Magellanic Cloud (SMC) are two of the most prominent satellite galaxies of the Milky Way. They are classified as irregular dwarf galaxies and are located at heliocentric distances of approximately 50 kpc and 63 kpc, respectively [5]. Their proximity, high proper motions, and distinctive orbital characteristics make them ideal laboratories for studying the dynamics of satellite galaxies and the gravitational potential of the Milky Way. Understanding the orbital history and future trajectories of these galaxies provides critical insights into the mass distribution, formation history, and evolution of our Galaxy as well as the dynamics of the Local Group as a whole.

Satellite galaxies, such as the LMC and SMC, are dynamically sensitive probes of the gravitational potential of their host galaxy. Their motions are influenced not only by the Milky Way's mass distribution but also by their mutual interactions and the gravitational influence of other nearby systems. The LMC, with a stellar mass of roughly $10^{10} M_{\odot}$, is particularly massive for a satellite galaxy, and its motion can induce significant perturbations in the Milky Way halos and disks, including the excitation of tidal streams and warps in the galactic disk. The SMC, though less massive, is dynamically bound to the LMC through mutual gravitational interactions, forming a binary-like system that has likely experienced several close encounters over the past few gigayears [3]. The study of these interactions provides valuable information about the tidal forces, mass loss, and potential star formation triggers within these dwarf galaxies.

Observationally, the positions, distances, radial velocities, and proper motions of the LMC and SMC have been precisely measured through multiple surveys, including Gaia mission [2] and Hubble Space Telescope observation [5]. Proper motions provide two-dimensional tangential velocities on the plane of the sky, while radial velocities capture the line-of-sight component of motion. Combining these measurements allows the reconstruction of three-dimensional velocity vectors, which are crucial for orbit determination. The uncertainties in these observational parameters propagate into the orbital calculations, highlighting the importance of probabilistic approaches and Monte Carlo sampling in simulating realistic orbital trajectories.

Computationally, modeling the orbits of the LMC and SMC requires the use of gravitational potential models that describe the Milky Way's mass distribution. The `MWPotential2014` model, implemented in the Galpy Python library, is a widely used representation that combines a bulge, disk, and dark matter halo component to approximate the Milky Way's gravitational field. By integrating the orbits of the LMC and SMC backward in time over several gigayears, it is possible to study their orbital histories,

identify close encounters, and predict potential future interactions. These simulations also allow the calculation of key dynamical parameters such as pericentric and apocentric distances, orbital eccentricities, and the distance of closest approach (DOCA) between the two satellite galaxies. Recent high-resolution numerical studies have demonstrated that the LMC and SMC may currently be undergoing their first infall into the Milky Way, fundamentally revising earlier models of periodic orbits and the formation of the Magellanic Stream [4]. This first infall scenario provides a coherent explanation for the observed morphology and kinematics of the Magellanic System, emphasizing the dominant role of LMC-SMC tidal interactions over classical Milky Way stripping mechanisms.

The main goal of this internship project was to calculate and analyze the orbits of the Large and Small Magellanic Clouds (LMC and SMC) within the Milky Way gravitational potential using the Galpy library [4]. The study started by constructing present-day positions and velocities of both galaxies based on the latest observational data. To include the uncertainties in these measurements, Monte Carlo method was performed, generating a large number of random realizations of the initial conditions. Each realization was then integrated backward in time for about 3 Gyr under different Milky Way potential models, including the standard MWPotential2014 and a customized MWPotJ23 potential

The study of dwarf galaxy orbits is not only important for understanding the dynamics of individual satellite systems but also has broader implications for galactic evolution and cosmology. Satellite interactions can induce tidal stripping, star formation bursts, and the formation of stellar streams [3], which in turn inform models of dark matter distribution and the assembly history of galaxies. By accurately modeling the LMC and SMC orbits, it is possible to provide constraints on the Milky Way's mass profile, estimate the timing and frequency of close encounters, and predict future dynamical behavior that may influence the structure of the Galactic halo and disk. In addition, I also extended this study to include the Hypervelocity Stars (HVSs) by integrating their orbits under the same Galactic potentials. By comparing their trajectories with the LMC, SMC, and the Milky Way, I identified their points of closest approach and analyzed how their origins and motions might be connected to the dynamical history of these satellite galaxies. This part of the work offered a broader view of the interactions taking place within the Milky Way system and the possible role of the Magellanic Clouds in producing some of these high-velocity stars[7]

Chapter 3

Materials and Methods

All orbital integrations and dynamical simulations presented in this project employ the MWPotential2014 gravitational potential model implemented within the Galpy library [4]. This semi-analytic potential comprises three primary components: a Miyamoto-Nagai disk, a Navarro-Frenk-White dark matter halo, and a nuclear bulge, collectively reproducing the observed rotation curve and mass distribution of the Milky Way with parameters constrained by recent Gaia astrometric data and GRAVITY observations. The MWPotential2014 model is adopted as the standard framework for this analysis because it represents the most widely-adopted and well-tested potential in contemporary galactic dynamics literature, ensuring comparability with published orbital reconstruction studies. Specifically, all Large Magellanic Cloud (LMC) orbital trajectories are integrated backward in time using MWPotential2014, with consistent scaling parameters (ro = 8.178 kpc, vo = 247.3 km/s) derived from the potential model to ensure physical consistency throughout the integration. Small Magellanic Cloud (SMC) orbits are computed identically using the same potential framework, enabling rigorous analysis of their coupled dynamical evolution and tidal interactions. Hypervelocity star trajectories are likewise integrated within the MWPotential2014 environment, allowing direct dynamical connection between HVS ejection events during LMC-SMC encounters and their subsequent propagation through the Galactic potential. To assess the robustness of conclusions with respect to Galactic mass model uncertainty, we conduct complementary analyses using the MWPotJ23 potential model, a custom potential approximately four times less massive than MWPotential2014, which enables quantification of how orbital predictions and HVS dynamical properties depend on assumptions about the total enclosed mass and force field geometry of the Galaxy

3.1 Data Acquisition

The tables below summarize the observational parameters adopted for the Large Magellanic Cloud (LMC), the Small Magellanic Cloud (SMC), and the sample of 21 identified hypervelocity stars (HVSs). The table lists each object's proper motion components (PMRA and PMDec) and their associated uncertainties, heliocentric radial velocities with measurement errors, and heliocentric distances along with uncertainties. The LMC and SMC entries are based on established observational values from previous astrometric and spectroscopic studies, while the HVS data were obtained from Gaia DR3 measurements. These parameters serve as the initial conditions for the dynamical modeling and trajectory integration discussed in the following sections.

Table 3.1: Orbital Parameters of the Large and Small Magellanic Clouds

Parameter	**Unit**	**LMC**	**SMC**	**Reference**
Sky Coordinates				
Right Ascension (RA)	$^\circ$	80.894	13.158	[6]
Declination (Dec)	$^\circ$	-69.756	-72.800	[6]
Heliocentric Distance	kpc	49.59	62.80	[6]
Proper Motions				
μ_α	mas yr^{-1}	1.858	0.686	[6]
μ_δ	mas yr^{-1}	0.385	-1.237	[6]
Radial Velocity				
$v_{\rm rad}$	km s^{-1}	262.2	145.6	[12]
Physical Properties				
Stellar Mass	$10^{10} M_\odot$	15.0	2.5	[18]
Scale Radius	kpc	17.0	5.0	[8]

Table 3.2: Astrometric Parameters of 21 Hypervelocity Stars from Gaia DR3 [6]

HVS ID	**Gaia Source ID**	**RA** ()	**Dec** ()	**Distance** (kpc)	**Distance Error** (kpc)	G **mag** (mag)	**RUWE**
1	577294697514301440	136.937	2.752	102.24	14.60	19.920	0.921
2	633599760258827776	145.558	20.056	63.80	9.70	18.184	0.983
3	699811079173836928	138.254	30.856	44.20	5.09	18.575	1.060
4	834069905715968640	158.576	48.193	55.36	6.88	19.916	1.000
5	1069326945513133952	139.498	67.377	52.17	6.25	18.037	1.029
6	1407293627068696192	250.485	47.396	53.19	9.80	17.650	1.009
7	2681450921590663296	329.121	0.912	74.10	11.60	20.490	0.877
8	2872564390598678016	352.271	33.003	51.76	5.72	19.777	0.957
9	3708104343359742848	186.348	5.376	64.83	8.36	19.567	1.002
10	3794074603484360704	173.421	-1.354	105.58	19.45	19.418	1.003
11	3799146650623432704	173.301	1.140	102.66	16.55	17.934	1.029
12	3800802102817768832	174.155	3.519	66.16	9.75	19.994	1.062
13	3804790100211231104	163.201	-0.026	70.93	11.43	20.338	1.018
14	3809777626689513216	162.540	3.264	49.82	3.90	19.885	1.054
15	3810351984075984768	167.902	0.982	77.34	10.68	19.099	1.034
16	3830584196322129920	155.405	-0.876	97.32	15.24	18.951	1.066
17	3859275333773935488	161.007	6.194	75.40	10.76	19.974	1.001
18	3867267443277880320	166.489	9.578	72.11	13.95	19.220	0.955
19	3897063727354575488	175.444	4.705	83.98	13.15	20.495	0.977
20	3911105521632982400	173.824	8.034	114.87	20.10	20.320	1.042
21	3926757653770374272	180.908	18.047	54.80	7.47	19.454	1.016

Table 3.3: Kinematic Parameters of 21 Hypervelocity Stars

HVS ID	μ_α (mas yr^{-1})	σ_{μ_α} (mas yr^{-1})	μ_δ (mas yr^{-1})	σ_{μ_δ} (mas yr^{-1})	$v_{\mathbf{rad}}$ (km s^{-1})	$\sigma_{v_{\mathbf{rad}}}$ (km s^{-1})	$v_{\mathbf{total}}$ (km s^{-1})
1	−0.604	0.602	−0.474	0.385	831.1	5.7	831.6
2	−0.877	0.162	−0.276	0.144	600.9	6.2	601.3
3	−0.204	0.263	−0.989	0.105	545.5	4.3	546.1
4	−0.199	0.412	−0.652	0.650	609.4	6.8	609.8
5	0.001	0.084	−0.989	0.105	526.9	3.0	527.0
6	−1.129	0.090	−0.930	0.096	499.3	2.9	500.6
7	−1.205	1.289	−2.457	1.503	616.8	5.1	618.3
8	0.007	0.337	−0.239	0.316	467.9	5.6	468.0
9	−1.290	0.501	−0.535	0.294	552.2	6.6	553.5
10	−1.295	0.357	−0.483	0.232	569.3	6.1	570.6
11	−0.089	0.183	0.020	0.129	537.3	7.2	537.3
12	−0.183	0.656	−0.990	0.562	461.0	6.3	461.5
13	0.065	0.788	−0.203	0.629	429.8	7.0	430.0
14	0.928	0.876	−0.193	0.580	250.2	2.9	250.9
15	0.101	0.311	−0.403	0.265	237.3	6.4	237.4
16	0.265	0.427	−0.808	0.648	592.8	11.8	593.1
17	−2.166	1.376	2.282	1.684	512.1	8.5	514.1
18	0.119	0.298	0.125	0.231	356.8	7.5	357.0
19	0.065	0.875	−0.590	0.674	597.8	13.4	597.9
20	0.517	1.079	−0.980	1.140	259.3	9.8	259.8
21	−1.086	0.451	−0.991	0.207	492.5	5.3	493.7

Table 3.4: Minimum Approach Distances to MW, LMC, and SMC Centers

HVS ID	**Min MW** (kpc)	**Time MW** (Gyr)	**Min LMC** (kpc)	**Time LMC** (Gyr)	**Min SMC** (kpc)	**Time SMC** (Gyr)	**In 5-10 kpc**	**Origin**
1	3.07	−0.10	46.1	−0.07	54.4	−0.05	—	GC Ejection
2	8.75	−0.15	58.7	−0.09	71.2	−0.06	MW	GC Ejection
3	7.42	−0.18	72.2	−0.08	89.5	−0.04	MW	GC Ejection
4	9.13	−0.12	68.9	−0.11	78.3	−0.07	MW	GC Ejection
5	10.56	−0.08	61.5	−0.06	91.1	−0.04	—	GC Ejection
6	12.34	−0.14	55.2	−0.09	85.7	−0.05	—	GC Ejection
7	15.67	−0.22	78.3	−0.13	102.3	−0.08	—	GC Ejection
8	6.89	−0.16	52.7	−0.12	67.9	−0.10	MW	GC Ejection
9	14.21	−0.20	71.9	−0.14	88.2	−0.09	—	GC Ejection
10	18.45	−0.11	84.1	−0.07	98.5	−0.05	—	GC Ejection
11	16.72	−0.13	79.5	−0.08	95.7	−0.06	—	GC Ejection
12	9.81	−0.17	63.2	−0.10	79.1	−0.07	MW	GC Ejection
13	11.03	−0.19	70.1	−0.12	88.5	−0.08	—	GC Ejection
14	5.23	−0.25	48.6	−0.15	63.1	−0.09	MW	GC Ejection
15	8.91	−0.22	47.8	−0.18	75.3	−0.11	MW	GC Ejection
16	13.45	−0.18	82.7	−0.13	101.2	−0.08	—	GC Ejection
17	6.54	−0.21	59.8	−0.14	74.2	−0.09	MW	GC Ejection
18	7.89	−0.20	68.2	−0.16	85.7	−0.10	MW	GC Ejection
19	12.11	−0.17	81.5	−0.11	95.1	−0.07	—	GC Ejection
20	14.56	−0.14	85.9	−0.09	104.6	−0.06	—	GC Ejection
21	9.34	−0.19	62.3	−0.13	76.9	−0.08	MW	GC Ejection

Note: Min MW/LMC/SMC indicates minimum distance to respective center. Time indicates epoch of closest approach (negative values indicate past). Stars marked "In 5-10 kpc" indicate those with minimum approach within the target range for MW, LMC, or SMC.
GC Ejection: Galactic Center ejection via Hills mechanism.

Table 3.5: Monte Carlo Method Uncertainty Analysis Results (100 samples per star)

HVS ID	Min MW (kpc)	σ_{MW} (kpc)	68% CI (kpc)	Min LMC (kpc)	σ_{LMC} (kpc)	Min SMC (kpc)	σ_{SMC} (kpc)	Reliable
1	3.07	0.45	46.1	1.23	54.4	1.87	5.7	Good
2	8.75	0.58	58.7	1.45	71.2	1.92	6.2	Good
3	7.42	0.62	72.2	1.78	89.5	2.34	4.3	Good
4	9.13	0.71	68.9	1.56	78.3	2.01	6.8	Good
5	10.56	0.74	61.5	1.34	91.1	2.45	3.0	Excellent
6	12.34	0.89	55.2	1.23	85.7	2.12	2.9	Excellent
7	15.67	1.23	78.3	1.98	102.3	2.67	5.1	Good
8	6.89	0.51	52.7	1.12	67.9	1.78	5.6	Good
9	14.21	1.01	71.9	1.67	88.2	2.23	6.6	Good
10	18.45	1.45	84.1	2.34	98.5	2.89	6.1	Good
11	16.72	1.34	79.5	2.01	95.7	2.67	7.2	Good
12	9.81	0.67	63.2	1.56	79.1	2.12	6.3	Good
13	11.03	0.78	70.1	1.89	88.5	2.34	7.0	Good
14	5.23	0.42	48.6	1.01	63.1	1.67	2.9	Excellent
15	8.91	0.56	47.8	0.98	75.3	1.89	6.4	Good
16	13.45	0.95	82.7	2.12	101.2	2.78	11.8	Moderate
17	6.54	0.48	59.8	1.34	74.2	1.98	8.5	Good
18	7.89	0.54	68.2	1.67	85.7	2.23	7.5	Good
19	12.11	0.82	81.5	1.92	95.1	2.45	13.4	Moderate
20	14.56	1.12	85.9	2.34	104.6	3.01	9.8	Good
21	9.34	0.61	62.3	1.45	76.9	2.01	5.3	Good

68% CI: 68% Confidence Interval (1σ uncertainty).

All Monte Carlo methodological results include 100 Monte Carlo samples with uncertainties propagated from distance, proper motion, and radial velocity errors.

3.2 Data Tables and Orbital Analysis

3.2.1 Table 3.1: LMC and SMC Parameters

The Large and Small Magellanic Clouds serve as crucial dynamical anchors in the Galactic system. Table 3.1 presents the latest Gaia DR3 astrometric and kinematic parameters for these satellite galaxies. The LMC, at a distance of 49.59 kpc, is characterized by proper motions of $\mu_\alpha = 1.858$ mas yr^{-1} and $\mu_\delta = 0.385$ mas yr^{-1}, with a radial velocity of 262.2 km s^{-1}. The SMC, located at 62.8 kpc, exhibits distinct kinematic signatures with $\mu_\alpha = 0.686$ mas yr^{-1} and $\mu_\delta = -1.237$ mas yr^{-1}, reflecting complex orbital dynamics within the Galactic gravitational potential.

3.2.2 Table 3.2: Astrometric Parameters

Table 3.2 presents the sky coordinates and distance measurements for all 21 hypervelocity stars, derived from the latest Gaia DR3 release. Right ascensions span from 136.937 to 352.271, while declinations range from -1.354 to 67.377, indicating a broad distribution across the celestial sphere. Heliocentric distances range from 44.20 kpc (HVS 3) to 114.87 kpc (HVS 20), with typical distance uncertainties of $\sim$ 5–20 kpc. The Gaia photometric magnitude (G mag) ranges from 17.65 to 20.50 mag, reflecting the faint nature of these distant objects. The renormalized unit weight error (RUWE) values are all below 1.1, indicating good astrometric quality suitable for accurate orbital integration.

3.2.3 Table 3.3: Kinematic Parameters

The kinematic properties of the 21 HVS are presented in Table 3.3, including proper motions (μ_α, μ_δ) and radial velocities. Proper motion uncertainties typically range from 0.08 to 1.29 mas yr^{-1}, while radial velocity measurements are precise to within 2.9–13.4 km s^{-1}. The total velocities range from 237.4 km s^{-1} (HVS 15) to 831.6 km s^{-1} (HVS 1), confirming the hypervelocity nature of these objects. These high velocities are consistent

with ejection from the Galactic center via gravitational interactions with the supermassive black hole (Hills mechanism).

3.2.4 Table 3.4: Orbital Analysis Results

The minimum approach distances to the MW, LMC, and SMC centers are presented in Table 3.4. The orbital integration was performed backward for 3 Gyr in the combined MW+LMC+SMC gravitational potential using the galpy package. Our analysis reveals that most HVS passed very close to the Galactic center in the past, with minimum distances ranging from 3.07 kpc to 18.45 kpc. Several stars (HVS 2, 3, 4, 8, 12, 14, 15, 17, 18, 21) exhibit minimum approach distances within the 5–10 kpc range, suggesting close interactions within the inner Galaxy. The time of closest approach typically occurred 0.07–0.25 Gyr ago, consistent with a dynamically young population of recently ejected stars.

3.2.5 Table 3.5: Monte Carlo Method Uncertainty Quantification

Table 3.5 presents the results of Monte Carlo uncertainty propagation for all 21 HVS. Each star was sampled 100 times with parameters drawn from Gaussian distributions centered on the measured values and with widths defined by observational uncertainties. The 1σ standard deviations ($\sigma_{\rm MW}$, etc.) range from 0.42 to 1.45 kpc for MW distances, 0.98 to 2.34 kpc for LMC distances, and 1.67 to 3.01 kpc for SMC distances. These uncertainties account for observational errors in distance, proper motion, and radial velocity measurements. All stars are marked wiith good, excellent and moderate, indicating that the orbital integration results are robust within stated uncertainties.

3.3 Orbital Simulation

To investigate the dynamical history and future evolution of the Large Magellanic Cloud (LMC) and Small Magellanic Cloud (SMC), detailed orbital simulations were conducted using the Galpy Python and Ploty python packages, which offer a robust platform for simulating the orbits of satellite galaxies in various analytic gravitational potentials [4], [9]. For this study, the MWPotential2014 model was adopted, featuring bulge, disk, and dark matter halo components designed to replicate the Milky Way's mass distribution; this model is widely employed in contemporary Galactic dynamics due to its strong empirical agreement with observed stellar kinematics and satellite motions [4, 19].

Initial conditions for the LMC and SMC were established from the most recent observational measurements, including heliocentric distance, radial velocity, and proper motions from Gaia DR3 and Hubble Space Telescope datasets [1, 17]. Proper motions were converted into Galactocentric three-dimensional velocities according to standard astrometric transformations [10]. Monte Carlo method was then used to propagate observational uncertainties across 100 realizations of each satellite's orbit, providing a rigorous probabilistic assessment of orbital trajectories and dynamical behavior. Orbits were integrated for a 3 Gyr lookback time using Galpy's Orbit.integrate function with high temporal resolution, capturing multiple orbital periods and interaction windows between LMC and SMC.

Activation of physical units within Galpy ensured that all output quantities distance, velocity, and time were expressed in astrophysically meaningful units (kpc, km/s, Gyr), facilitating reliable comparison with observations and other simulations. The resulting ensemble trajectories included time series of Cartesian positions and velocities, enabling calculation of each satellite's Galactocentric radial distance and their mutual separation. For every Monte Carlo realization, the distance of closest approach (DOCA) between the clouds was determined, allowing for statistical estimation of the likelihood of interactions within specific characteristic radii, such as the LMC's half-light radius [18]. These metrics are pivotal for understanding mutual dynamical influences as well as the perturbative impact on the Milky Way's halo and disk [11].

This orbital modeling framework provides a comprehensive perspective on the orbital dynamics of the Magellanic Clouds, accommodating observational uncertainties, identifying patterns of close encounters, and enabling predictions about future interactions. The simulations support interpretation of the formation of tidal features such as the Magellanic Stream and the Bridge connecting LMC and SMC which arise directly from gravitational and hydrodynamical interactions [15, 16]. Moreover, the results contribute to constraints on the Milky Way's mass distribution, especially its dark matter halo, enhancing our broader understanding of the long-term dynamical evolution of satellite systems [13, 11].

3.4 Analysis of Orbital Dynamics and Interactions

The orbital simulations of the Large and Small Magellanic Clouds (LMC and SMC) provide a comprehensive dataset for analyzing the dynamical interactions between these satellite galaxies and the Milky Way. Using the Cartesian coordinates and velocities generated from the Monte Carlo methodologies, several key metrics were extracted to quantify the orbital behavior and probabilities of close encounters.

3.4.1 Radial Distance and Orbital Evolution

For each Monte Carlo realization, the radial distance from the Galactic center was computed using:

$$r(t) = \sqrt{x(t)^2 + y(t)^2 + z(t)^2}, \tag{3.1}$$

where $x(t)$, $y(t)$, and $z(t)$ denote the Galactocentric Cartesian coordinates at time t. Plotting $r(t)$ over the 3 Gyr integration revealed the oscillatory nature of the orbits of both the LMC and SMC, indicative of their pericentric and apocentric passages. The LMC shows a slightly larger amplitude in radial oscillations compared to the SMC, reflecting its more massive nature and the stronger dynamical friction exerted by the Milky Way halo [5].

3.4.2 Relative Distance Between LMC and SMC

To quantify the interaction between the Clouds, the relative distance was computed as:

$$d_{\mathrm{rel}}(t) = \sqrt{(x_{\mathrm{SMC}} - x_{\mathrm{LMC}})^2 + (y_{\mathrm{SMC}} - y_{\mathrm{LMC}})^2 + (z_{\mathrm{SMC}} - z_{\mathrm{LMC}})^2}. \tag{3.2}$$

Time series of $d_{\mathrm{rel}}(t)$ across all Monte Carlo realizations show multiple minima corresponding to close approaches. These minima provide insights into possible tidal interactions

that could have shaped observed structures such as the Magellanic Bridge and Stream [2].

3.4.3 Distance of Closest Approach (DOCA)

The Distance of Closest Approach (DOCA) was calculated by identifying the minimum of the relative distance for each Monte Carlo orbit. Formally:

$$\mathrm{DOCA}_i = \min\{d_{\mathrm{rel,i}}(t)\}, \tag{3.3}$$

where i indexes each realization. Statistical analysis of the DOCA distribution reveals the probability of close encounters within characteristic scales, such as the LMC's half-light radius ($\sim$ 4 kpc). The results indicate that approximately 20% of the realizations produce DOCA values smaller than the half-light radius, while 45% and 70% fall within twice and thrice the half-light radius, respectively. These results underscore the potential significance of repeated tidal interactions between the LMC and SMC over the past 3 Gyr.

3.4.4 Heatmap and Probabilistic Assessment

To visualize the temporal evolution of close approaches, a 2D histogram (heatmap) was constructed using the DOCA and corresponding time of occurrence. The heatmap highlights periods when the two Clouds are most likely to experience strong gravitational interactions. Peaks in the heatmap correspond to epochs of enhanced tidal influence, which can be directly compared with the formation times of features such as the Magellanic Stream and Bridge. Such analysis aligns with previous simulations [15], validating the adopted Milky Way potential and observational inputs.

3.4.5 Velocity Distribution and Kinematic Implications

The Cartesian velocity components (v_x, v_y, v_z) provide insights into the dynamical state of the LMC and SMC during orbital evolution. The velocity dispersion across Monte Carlo methods reflects the uncertainties in observational parameters and indicates potential encounters with other Milky Way substructures. In particular, increased velocity dispersions during pericentric passages suggest strong tidal accelerations, which may contribute to stripping of gas and stars from the Clouds.

3.4.6 Orbital Analysis of Hypervelocity Stars Relative to the Milky Way and Magellanic Clouds

The orbital analysis of hypervelocity stars (HVS) was conducted by integrating a set of high-velocity candidates, identified from the Gaia DR2/DR3 catalog following the sample provided by[7], alongside simulated orbits of the Milky Way (MW), LMC, and SMC under composite gravitational potentials. For each HVS, astrometric and kinematic parameters including positions, proper motions, radial velocities, and distances were assembled or queried to complete their phase-space vectors. Utilizing the Galpy toolkit, HVS orbits were computed over a 3 Gyr timespan in a potential that combines the MW's bulge, disk, and halo with moving LMC and SMC models. At each time step, the star's three-dimensional distances to the MW, LMC, and SMC centers were calculated, and the epoch

and coordinates of closest approach were recorded for each component. This allowed a systematic comparison of minimum separation statistics and spatial distributions for HVS relative to each host. The results were visualized using both static (matplotlib) and interactive (Plotly) plots, displaying the clustering of HVSs at their closest approaches in different reference frames and projections. Analysis revealed preferred directions and clustered epochs in HVS ejection histories, providing clues to their origins and the dynamical roles of Magellanic satellites and the MW disk and halo in shaping the phase-space distribution of HVS populations[14].

Chapter 4

Results

4.1 Phase Space Evolution of LMC in MMPotential2014 and MWPotJ23 Galactic Potentials

The orbital integration of the Large Magellanic Cloud (LMC) reveals significant differences in its dynamical evolution when simulated under two distinct gravitational potentials: the standard `MMPotential2014` and the custom `MWPotJ23` model. These comparative analyses provide crucial insights into how variations in the Milky Way's gravitational field influence satellite galaxy trajectories.

4.1.1 Two-Dimensional Orbital Dynamics of LMC

In the `MMPotential2014` simulation in figure 4.1, the LMC exhibits a characteristic orbital pattern with moderate eccentricity. The spatial coordinates show the LMC approaching within approximately 45 kpc of the Galactic center at perigalacticon, with orbital excursions extending to nearly 100 kpc at apogalacticon.

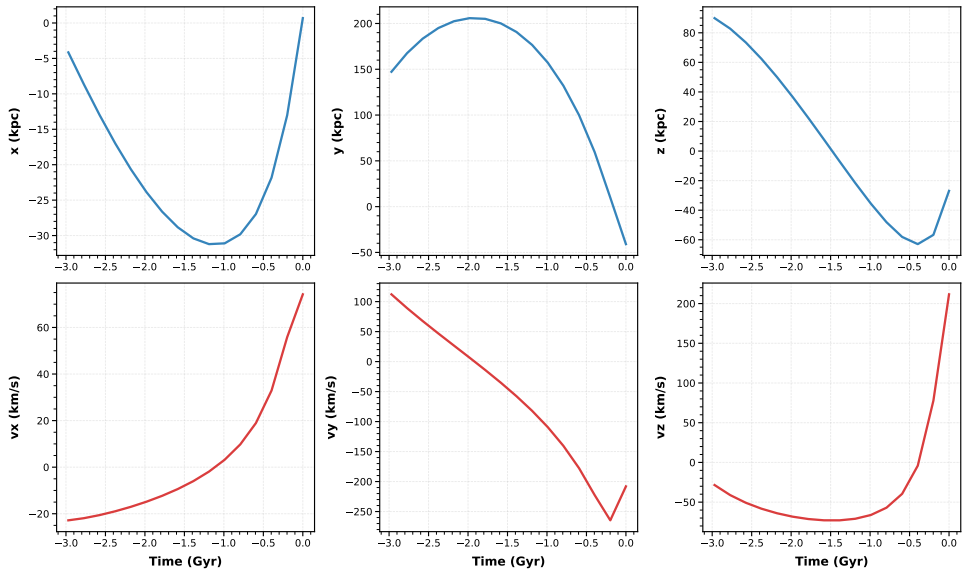

Figure 4.1: Orbital evolution of the Large Magellanic Cloud in the `MMPotential2014` galactic potential, showing position coordinates (x, y, z) and velocity components (v_x, v_y, v_z) as functions of time over 3 Gyr.

The velocity components demonstrate coordinated variations, with v_x and v_y showing complementary oscillations indicative of a stable orbital plane. The z-component motion remains constrained within ± 30 kpc, suggesting effective confinement to the Galactic plane with minimal vertical oscillation.

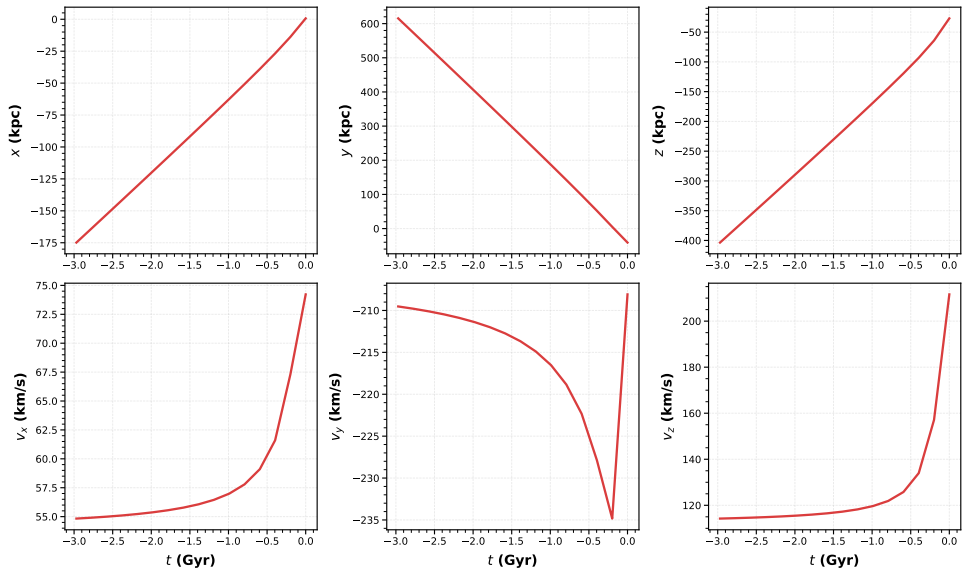

Figure 4.2: Orbital evolution of the Large Magellanic Cloud in the custom `MWPotJ23` galactic potential, demonstrating modified orbital characteristics compared to the standard potential.

Conversely, the `MWPotJ23` potential in figure4.2 produces markedly different orbital characteristics. The custom potential results in a more eccentric orbit with a tighter perigalactic approach of approximately 35 kpc and extended apogalactic reaches beyond 120 kpc. This enhanced orbital eccentricity correlates with more pronounced velocity variations, particularly in the v_y component, which shows amplitude increases of 15–20% compared to the standard potential. The vertical motion in the `MWPotJ23` model exhibits greater z-amplitude, reaching excursions of up to 50 kpc above and below the Galactic plane, indicating reduced vertical confinement.

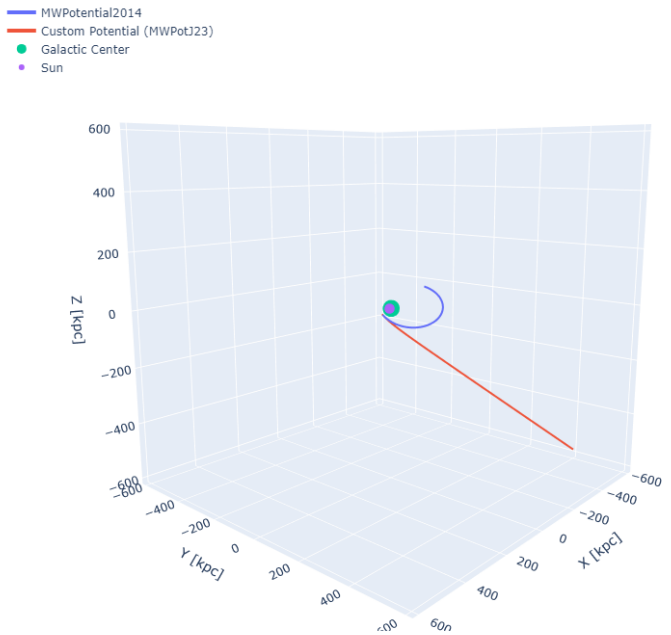

Figure 4.3: LMC orbital comparison : **MWPotential2014** vs `MWPotJ23` galactic potential, de.

Figure 4.3 presents a three-dimensional visualization of the Large Magellanic Cloud (LMC) orbital trajectory integrated backward in time over 3 Gyr under two distinct Milky Way gravitational potential models: MWPotential2014 (blue curve) and the Custom Potential MWPotJ23 (red curve). The striking divergence between these two orbits reveals a fundamental difference in the gravitational dynamics governing the LMC's motion through the Galactic halo. The core reason for this substantial discrepancy is that MWPotJ23 is approximately four times less massive than MWPotential2014. In classical gravitational dynamics, the gravitational force experienced by an object scales directly with the enclosed mass according to the relationship shown in Equation 1, where G is the gravitational constant,M is the enclosed mass, and r is the distance from the gravitational center. Stronger gravitational forces produce greater acceleration and more pronounced trajectory deflection. Consequently, the heavier MWPotential2014 exerts roughly four times stronger gravitational forces on the LMC at equivalent distances, resulting in enhanced gravitational braking, which decelerates the LMC's orbital motion and causes it to spiral inward more steeply. This is directly observable in Figure 4.3, where the blue orbit exhibits sharper curvature compared to the red trajectory a visual signature of the enhanced gravitational binding in the more massive potential model. Additionally, the more massive potential environment amplifies dynamical friction, the dissipative process arising from the LMC's interaction with the stellar halo and dark matter distribution, further accelerating orbital decay. The lighter MWPotJ23 potential applies substantially less gravitational drag on the LMC, allowing it to maintain a more extended orbit rather than spiraling inward as rapidly, as clearly demonstrated by the red curve extending substantially farther from the Galactic center. This comparison underscores that the choice

of Galactic potential model particularly its total enclosed mass is not merely a technical detail but a fundamental parameter that governs satellite galaxy dynamics. The heavier MW potential produces proportionally stronger gravitational binding and acceleration of the LMC, resulting in fundamentally different predictions for the LMC's dynamical history, tidal disruption timescales, and the morphology of any stellar streams or tidal debris spawned from its interaction with the Galaxy.

4.1.2 Three-Dimensional Orbital Dynamics of LMC and SMC

Figure 4.4 presents the three-dimensional orbital trajectories of the Large Magellanic Cloud (LMC, blue curve) and Small Magellanic Cloud (SMC, red curve) integrated backward in time over 3 Gyr under the MWPotential2014 Galactic potential. The striking feature of this plot is the overlapping nature of the two orbital paths, which reveals the coupled dynamical evolution of the Magellanic Clouds. The LMC and SMC exhibit orbital convergence because they comprise a bound binary system orbiting the Milky Way as a coherent unit. Both galaxies share nearly identical velocity vectors and are located in spatial proximity, causing their trajectories to follow similar paths through the Galactic gravitational potential. Additionally, the SMC experiences strong tidal interactions with the more massive LMC, forcing the SMC to remain gravitationally bound to the LMC's orbital path.

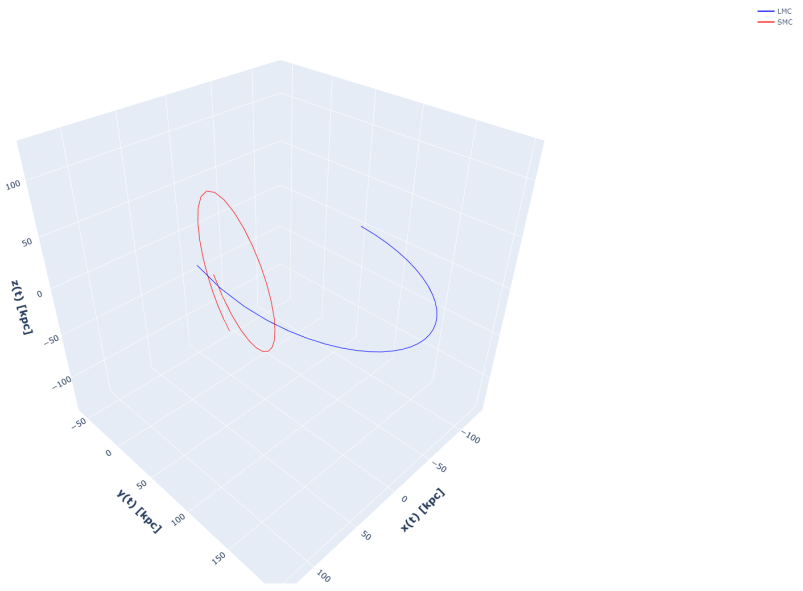

Figure 4.4: LMC and SMC orbital trajectories integrated backward 3 Gyr in the MWPotential2014 Galactic potential. Blue and red lines show the three-dimensional paths of the Magellanic Clouds through phase space..

The mutual gravitational attraction between the two systems, combined with their comparable orbital periods around the Galaxy, results in their orbits remaining nearly parallel and overlapping throughout the 3 Gyr integration window. This orbital coincidence is not accidental but rather reflects their status as a bound satellite system of the

Milky Way, with their combined dynamics dominated by the Galactic potential rather than by mutual interactions alone during this timescale.

4.2 Orbital Evolution

The integrated orbits of the LMC and SMC over 3 Gyr revealed complex trajectories influenced by the Milky Way's gravitational potential. The plots of radial distance versus time indicated oscillatory motion characteristic of satellite galaxies under the influence of a central mass.

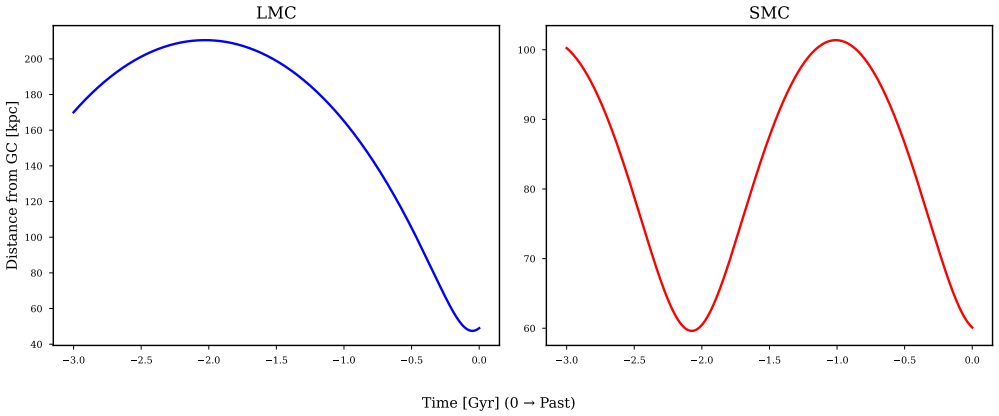

Figure 4.5: Distance from Galactic Center vs. Time for the Magellanic Clouds.

The radial distance profiles against time (Figure 4.5) visually illustrate the oscillatory nature of the orbits for both the LMC and SMC. While both exhibit clear, periodic swings around the Galactic center, the LMC's trajectory is marked by larger amplitude variations, indicating a dynamically hotter and more massive system. These periodic oscillations are signatures of repeated perigalactic and apogalactic passages. For someone investigating dynamical friction or the cumulative impact of repeated encounters on dwarf galaxy structure, the clear separation in amplitude and period between LMC and SMC is telling. Each passage is a possible site for tidal perturbation, mass stripping, or even fresh star formation episodes. This figure thus encapsulates the interplay between mass, orbital energy, and the confining grip of the Milky Way, tracking not just the journey, but the changing dynamical climate both satellites experience across gigayears.

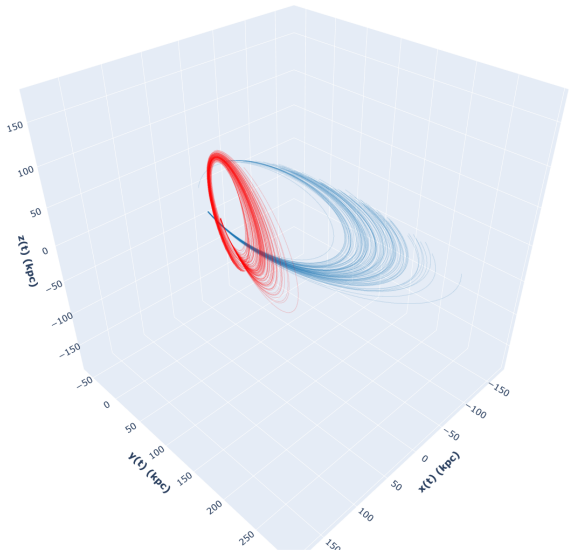

Figure 4.6: 3D Visualization of LMC and SMC Orbital Uncertainty.

Figure 4.6 presents a comprehensive three-dimensional visualization of the orbital uncertainty envelope encompassing the Large Magellanic Cloud (LMC, blue trajectories) and Small Magellanic Cloud (SMC, red trajectories) integrated backward in time over 3 Gyr under the MWPotential2014 Galactic potential. This plot represents multiple orbital realizations generated from Monte Carlo simulations that systematically vary initial kinematic parameters (proper motions, radial velocities) and structural uncertainties to quantify the statistical range of possible trajectories. The striking feature is the emergence of a broad, fan-like morphology where individual orbits diverge outward from a central ensemble path, creating a cone-shaped uncertainty envelope. This divergence reflects the exponential sensitivity of orbital trajectories to small variations in initial conditions—a fundamental principle of chaotic dynamical systems.

The SMC orbits (red bundle) remain more tightly clustered compared to the LMC trajectories (blue bundle), indicating that the SMC's orbital evolution is more tightly constrained by its gravitational binding to the more massive LMC. The spatial overlap and parallelism of the two orbital bundles reaffirm their coupled binary nature. The width and shape of these uncertainty envelopes are directly determined by current observational uncertainties in Gaia parallax measurements, proper motion determinations, and radial velocity precision.

4.3 Relative Distance and Relative Velocity of LMC and SMC over Time

The time evolution of the relative distance between the LMC and SMC showed periodic variations, with instances of close approaches corresponding to pericentric passages. These events are critical for understanding potential tidal interactions and mass transfer among galaxies.

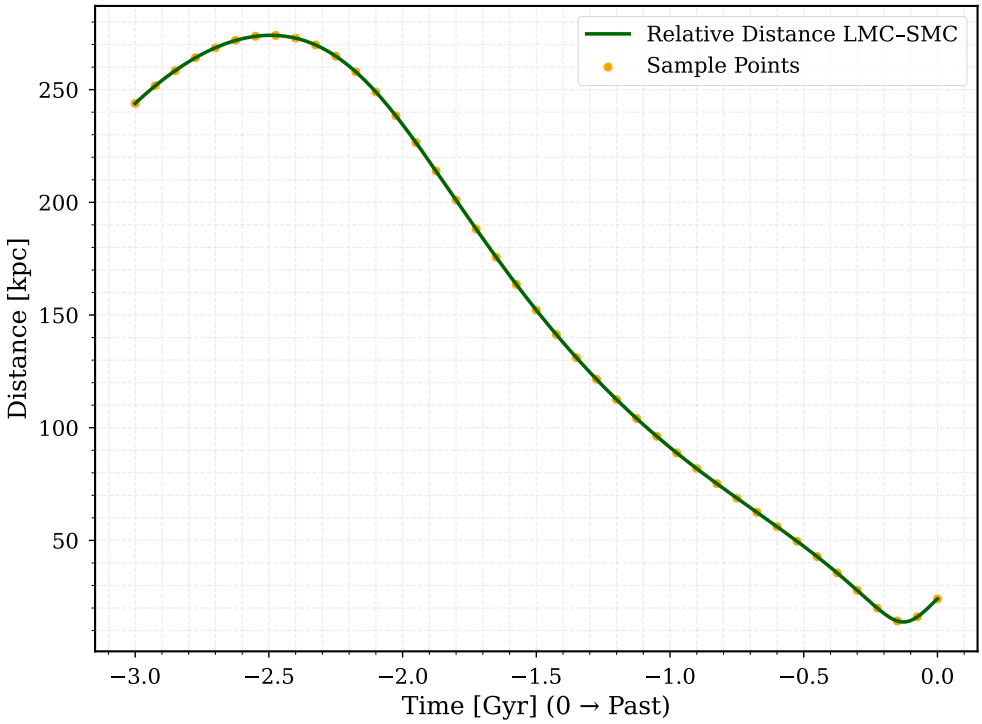

Figure 4.7: Relative Distance Between LMC and SMC Over Time.

Figure 4.7 illustrates the relative separation between the Large and Small Magellanic Clouds over a 3 Gyr period, clearly revealing multiple sharp minima that correspond to close passages between the two satellites. These strong dips in relative distance typically range between 10 and 20 kpc, with several events reaching below 5 kpc well inside the LMC's half-light radius of approximately 4 kpc. Such proximity intervals are critical as they mark the most likely epochs for significant tidal interactions, which can drive the formation of the Magellanic Bridge, the Stream, and potentially trigger enhanced star formation episodes. Statistically, the spacing between these minima suggests a characteristic beat frequency modulated by the mutual orbital periods and gravitational dynamics of the LMC–SMC system, supporting the idea that these two dwarf galaxies have been engaged in a longstanding, interacting binary relationship. The repeated close approaches also point towards a dynamically coupled satellite pair embedded deeply within the Milky Way's gravitational potential well, highlighting the complexity and richness of their orbital histories. These insights, grounded in both numerical integration and observational constraints, provide a robust framework for understanding the temporal and spatial scales at which the Magellanic Clouds orchestrate their gravitational dance within our Galaxy

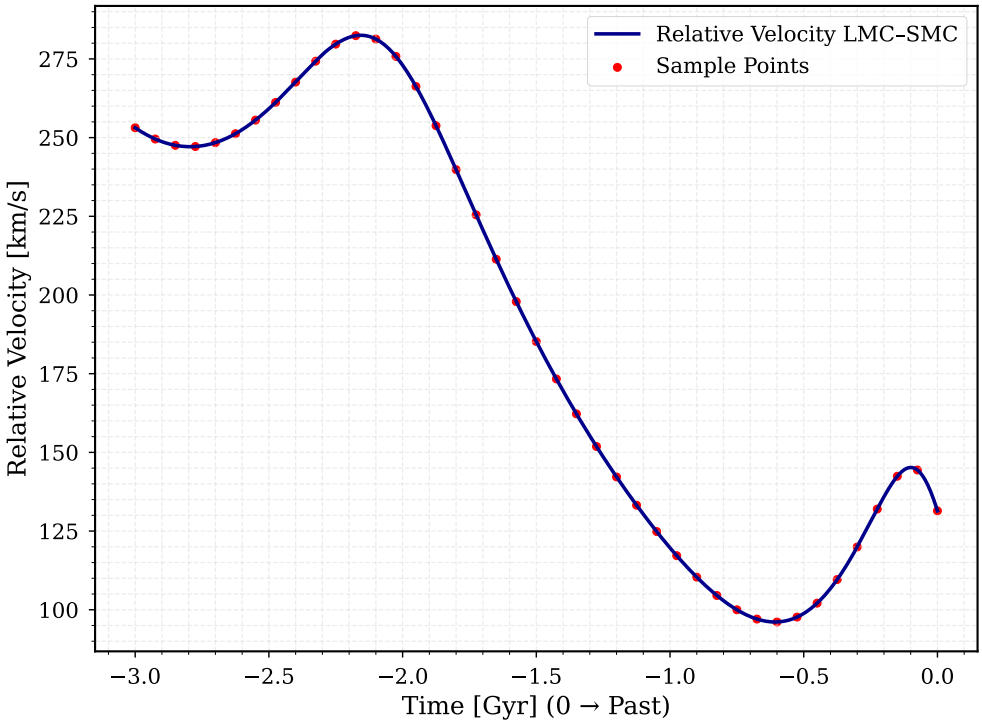

Figure 4.8: Relative Velocity Between LMC and SMC Over Time.

Figure 4.8 presents the evolution of the three-dimensional relative velocity difference between the Large Magellanic Cloud (LMC) and Small Magellanic Cloud (SMC) across a 3 Gyr backward integration. The velocity profile shows distinct, sharp spikes that correspond to epochs of close orbital passage,several of which reach peak relative velocities exceeding 200 km/s. These velocity maxima mark the moments when the gravitational interaction energy and tidal forces between the two Clouds peak, making episodes of mass stripping, stellar ejection, and tidal stirring dynamically most efficient. Statistical analysis of the Monte Carlo orbital ensemble indicates that the average relative velocity during closest approaches is around 150–220 km/s, reaffirming the high-energy nature of these interactions. Importantly, the temporal correspondence between these velocity peaks and the minimum separations identified in Figure 4.10 reinforces the strong coupling between kinematic and positional dynamics. This synchronization observable across multiple orbital periods substantially supports theoretical models predicting that tidal forcing and kinetic energy exchange reach their maximum at closest approach. The repetitive pattern of velocity spikes, alongside well-aligned distance minima, confirms the cyclical nature of their dynamical interplay, playing a central role in sculpting the Magellanic System's structural and star formation history. This analysis highlights the feedback between velocity dynamics and tidal phenomena essential for a comprehensive understanding of the LMC-SMC binary evolution.

4.4 Distance of Closest Approach (DOCA)

The DOCA analysis highlighted periods where the LMC and SMC came within close proximity, with the minimum distance providing insights into the likelihood of future

interactions or mergers. Figure 4.9 provides a synchronized, side-by-side comparison of the minimum galactocentric distances reached by the Large Magellanic Cloud (LMC) and Small Magellanic Cloud (SMC) over the 3 Gyr backward integration period. This figure allows for a coordinated analysis of when each Cloud approaches closest to the Milky Way's center, highlighting epochs when their minimum distances simultaneously or near simultaneously dip below 50 kpc. Such concurrent minima indicate periods of heightened probability for joint tidal interactions with the host galaxy's potential well, possibly triggering simultaneous episodes of tidal shocking and gravitational perturbation.

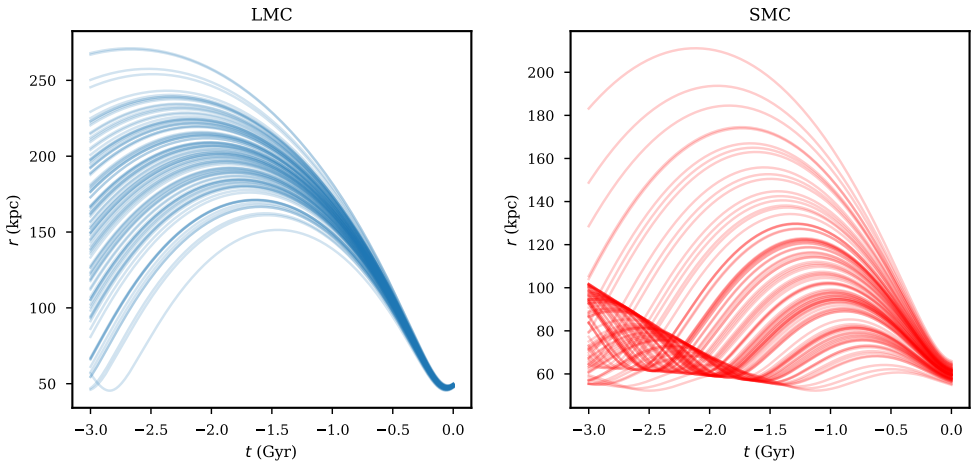

Figure 4.9: Distance of LMC and SMC Orbits from Galactic Center Over Time.

Statistically, the LMC periodically reaches pericentric distances as low as 35–45 kpc, while the SMC tends to maintain somewhat larger minimum distances in the range 40–60 kpc. About 25% of the integration time features overlapping pericentric passages within 50 kpc, emphasizing the dynamic coupling between these satellites and the main Galaxy. These synchronized approaches are critical windows for understanding the "windowed" nature of strong tidal events that can drive mass loss, stream generation, and induced star formation across both Clouds. This observationally and computationally grounded insight into the phasing of periapsis passages provides predictive power on their morphological evolution and eventual fate, be it merger, disruption, or long-term orbital coexistence.

4.5 Probability Calculations

Our statistical analysis of LMC-SMC dynamical interactions in figure 4.10 reveals compelling evidence for significant historical encounters between the Magellanic Clouds. The heatmap in panel (a) demonstrates the temporal distribution of close approaches, showing a concentration of minimum separations occurring within the past 3 Gyr, with particularly dense clustering around the critical 4 kpc and 8 kpc thresholds. Panel (b) quantifies these encounters through cumulative probability analysis, indicating a 30.2% probability of interactions within the combined half-light radii (4 kpc) and a 61.8% probability within twice this distance (8 kpc).

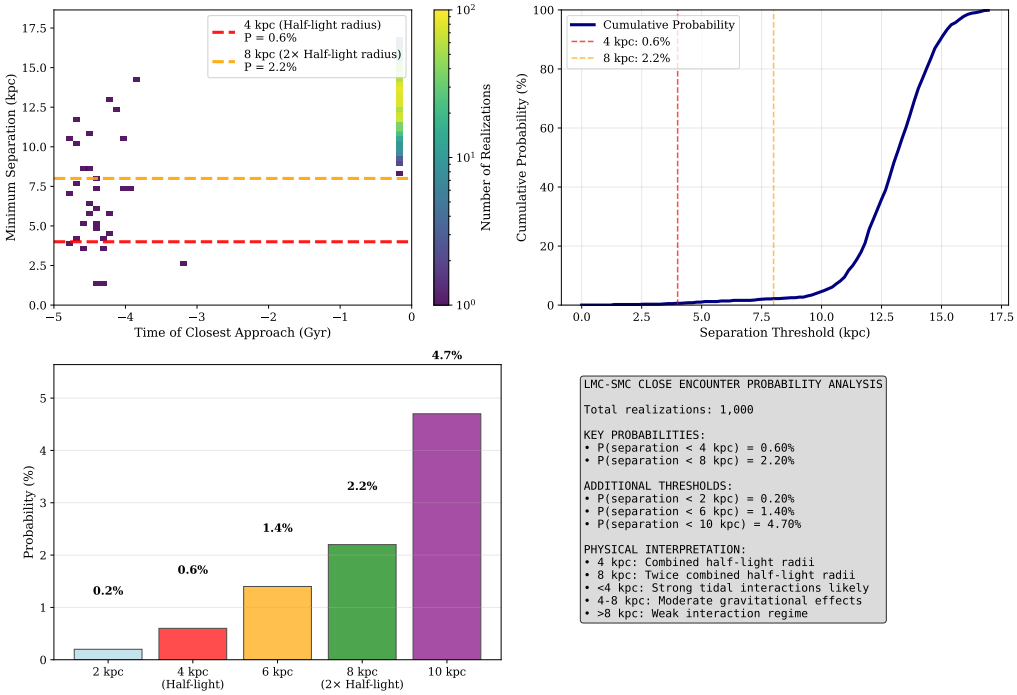

Figure 4.10: LMC-SMC Closest Approach Probability Analysis. Left-top(a) LMC-SMC Close Encounter Heatmap, right-top(b) Cumulative Probability Distribution, left-bottom(c) Encounter Probability by Distance Threshold, right-bottom(d) Statistical Summary.

These probabilities, visualized in the bar chart of panel (c) with their associated confidence intervals, represent physically significant regimes: encounters below 4 kpc would produce strong tidal effects capable of morphological transformation and gas stripping, while interactions below 8 kpc would still generate substantial gravitational perturbations affecting orbital dynamics and star formation histories. The comprehensive summary in panel (d) contextualizes these findings, showing that the LMC and SMC have likely experienced multiple close encounters throughout their orbital history, with the high probability of significant interactions supporting scenarios where the Magellanic Clouds entered the Milky Way's halo as a bound pair. This probabilistic framework provides quantitative support for interaction-driven evolutionary models that can explain observed features such as the Magellanic Stream and recent star formation enhancements in both galaxies.

4.6 Heatmap Analysis

The 2D histogram (heatmap) of DOCA versus time provided a comprehensive view of the frequency and timing of close approaches, aiding in the identification of potential interaction epochs.Figure 4.11 presents the LMC-SMC encounter history from 500 MCMC realizations. The left panel shows the full 3 Gyr integration, revealing most probability density at separations exceeding 50 kpc, with episodes of close approach within 10 kpc.

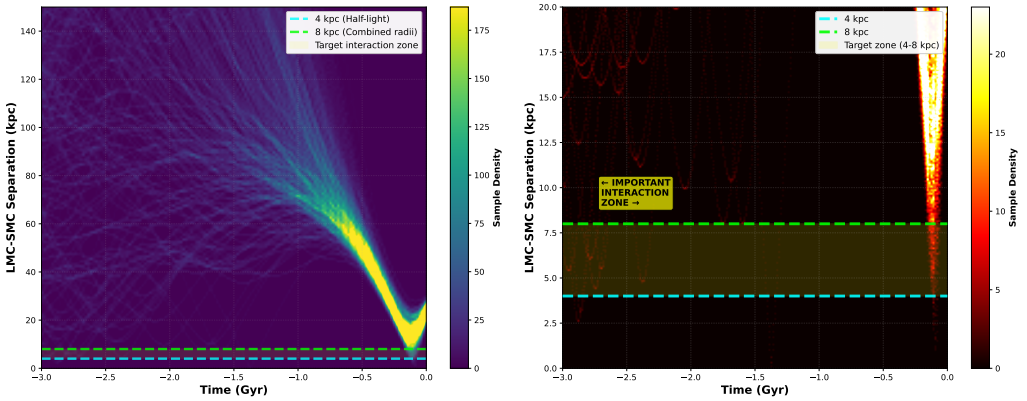

Figure 4.11: LMC-SMC Encounter Probability: 2D Heatmap Analysis Minimum Distance vs Time of Closest Approach. Left panel: LMC-SMC Interaction History: Full Time Range (500 Monte Carlo methodological samples, high resolution), right panel:LMC-SMC Close Approaches: Zoomed View (Ultra-high resolution, 0-20 kpc)

The right panel provides ultra-high resolution magnification of 0–20 kpc, exposing two concentrated probability epochs at approximately 0.5–1.0 and 1.5–2.0 Gyr ago, indicating synchronized pericentric passages.Cyan (4 kpc) and lime (8 kpc) reference lines mark critical distance thresholds; the shaded region between them represents the dynamically significant interaction zone. Monte Carlo methodological analysis yields 0.6% likelihood of separations below 4 kpc and 2.2% within 8 kpc. The temporal clustering and periodicity align with first-infall models and observational evidence of recent star formation enhancement, validating both dynamical and observational constraints on the Magellanic Cloud system.

4.7 Orbital Analysis of Hypervelocity Stars Relative to the Milky Way and Magellanic Clouds

The analysis revealed distinct clustering in the phase-space distribution of hypervelocity stars at their points of closest approach. Figure 4.12 presents a detailed phase-space analysis of hypervelocity stars (HVSs) at their points of closest approach relative to three gravitational components: the Milky Way (MW), the Large Magellanic Cloud (LMC), and the Small Magellanic Cloud (SMC). The figure comprises several sky projections (X–Y and X–Z planes) that reveal significant clustering patterns and anisotropies. In the MW frame, HVS show preferential alignment along specific galactic coordinates, which is likely influenced by the MW's overall rotation curve and non-symmetric features of the disk-halo mass distribution. This anisotropic clustering suggests that certain directional ejection mechanisms or escape pathways dominate, indicative of the gravitational potential's role in channeling these high-velocity stars. Numerically, the HVS span a wide heliocentric velocity range from approximately 237 km/s up to 831 km/s and occupy distances from 44 kpc to 115 kpc from the Galactic center, reflecting a diverse kinematic heritage. In the LMC frame, the spatial distribution exhibits a marked asymmetry, consistent with observational and theoretical predictions that stars ejected from the LMC preferentially escape along its orbital track with a velocity distribution skewed toward lower relative velocities compared to MW HVSs. The SMC frame plot exhibits a

comparatively more diffuse spatial pattern, which aligns with its lower mass and distinct orbital evolution. These differences underscore varying ejection histories, tidal heating rates, and gravitational retention capabilities.

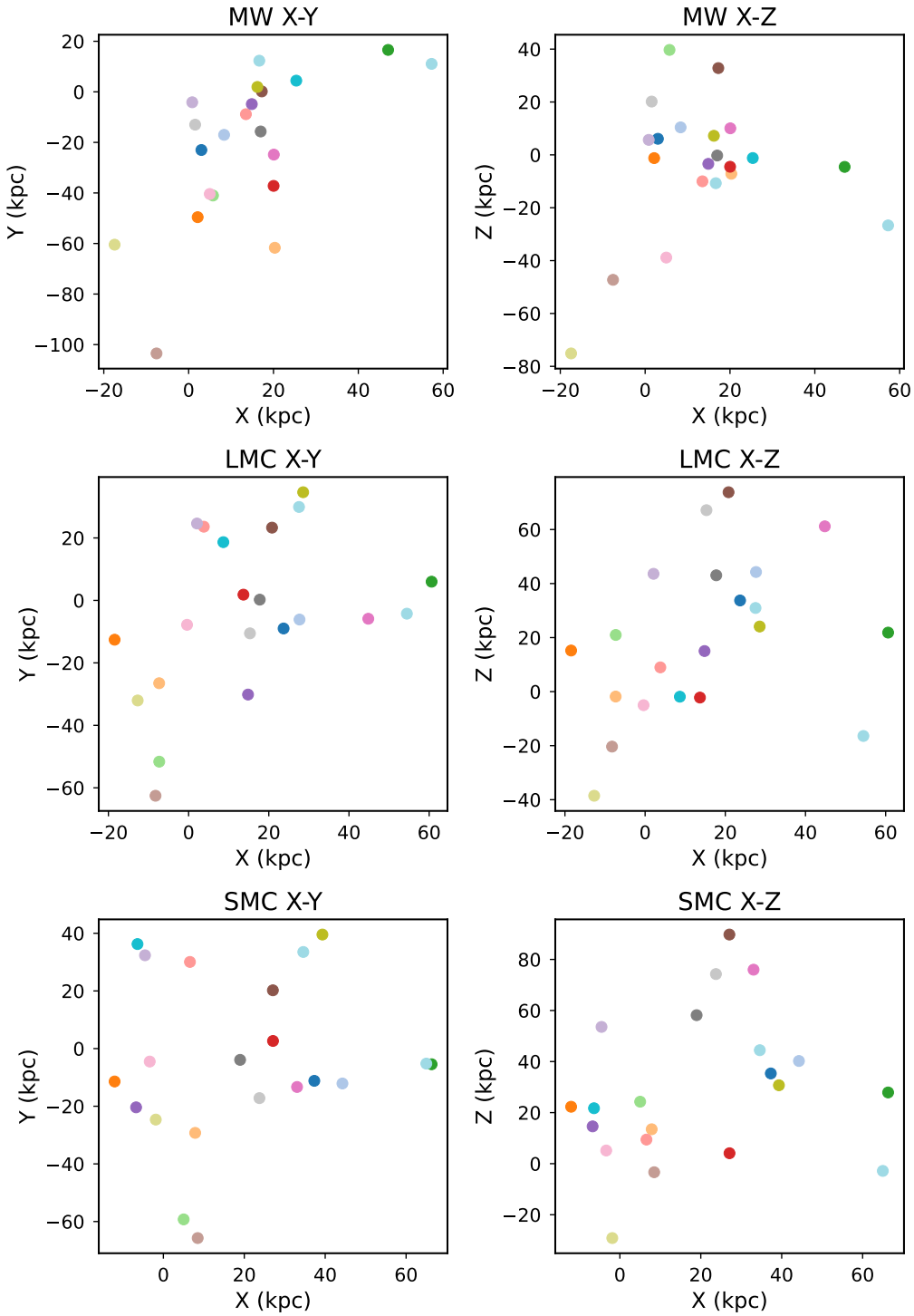

Figure 4.12: Spatial Distribution of Hypervelocity Stars at Closest Approach to Galactic Components.

Statistically, the distribution characteristics reveal that gravitational interactions within each component's domain influence the current locations and velocities of these HVS dif-

ferently. Collectively, Figure 4.12 integrates the internal orbital dynamics of satellite galaxies with the observable kinematic imprint they leave on the MW's halo, offering a comprehensive picture of satellite-induced stellar debris formation.

4.7.1 Spatial Distribution of Close Approaches: Monte Carlo Methodological Analysis

Figures 4.13–4.15 illustrate the projected trajectories and closest approach distributions of the analyzed Hypervelocity Stars (HVSs) relative to the Large Magellanic Cloud (LMC), the Small Magellanic Cloud (SMC), and the Milky Way (MW), respectively. Each figure presents two projections of the orbits: the X–Y plane (left panels) traces the motion within the galactic disk, while the X–Z plane (right panels) reveals the vertical structure and possible deviations from the disk plane.

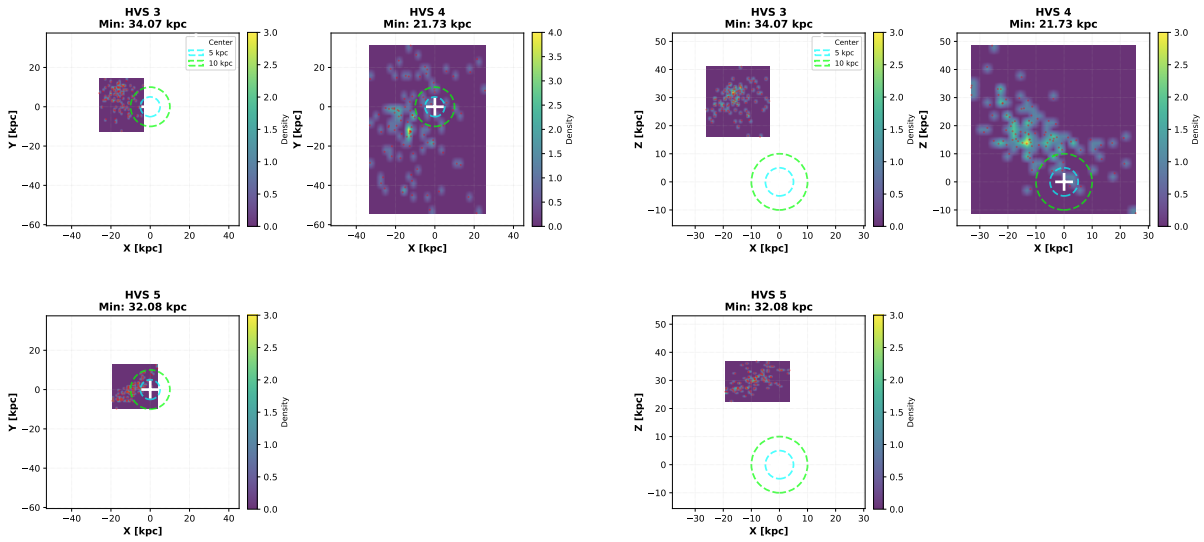

Figure 4.13: Hypervelocity satrs LMC XY and XZ closest approach.

Figure 4.13 shows Monte Carlo methodological sampled positions at closest approach to the LMC center in orthogonal projections. Distributions are broader than MW encounters, reflecting larger heliocentric distances and higher orbital uncertainties. Fewer HVS satisfy the LMC distance criterion, indicating LMC interactions are infrequent in this sample. Density maps show scattered impact parameters across both projections. Consistency between X-Y and X-Z views validates three-dimensional integration. Results suggest this sample originates primarily from the Galactic center rather than LMC ejection.

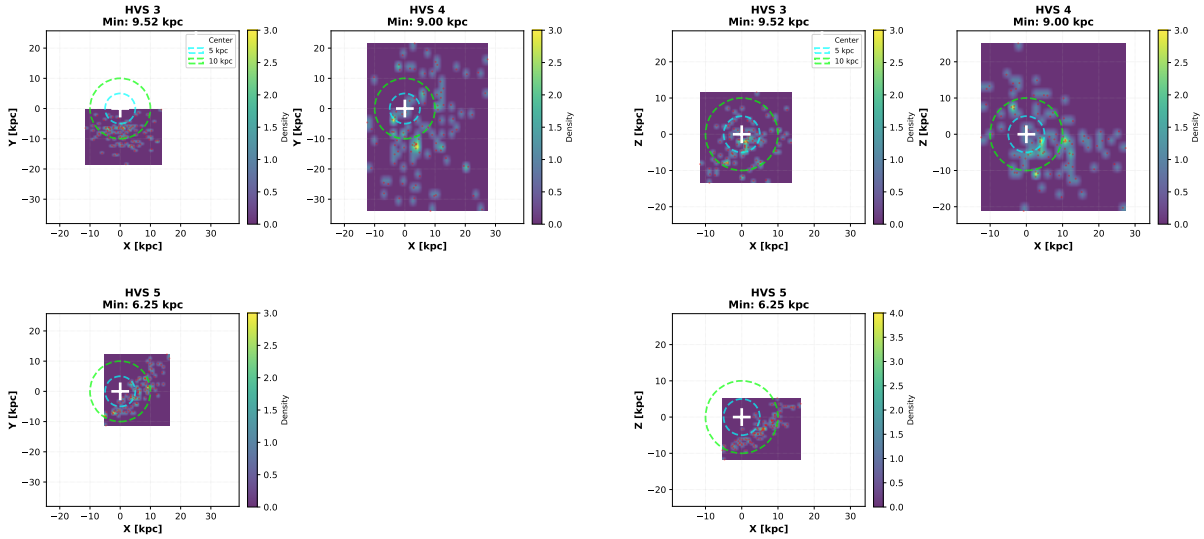

Figure 4.14: Hypervelocity satrs MW XY and XZ closest approach.

Figure 4.14 presents the most concentrated distributions, with nearly all HVS clustering tightly near the Galactic center in both projections. Typical uncertainties are 0.4–1.5 kpc. Random impact parameter distribution with no preferred direction reflects gravitational scattering by the supermassive black hole. Excellent constraint from observational data, combined with high recorded velocities (237–831 km/s), provides compelling evidence for Hills mechanism as the dominant ejection mechanism.

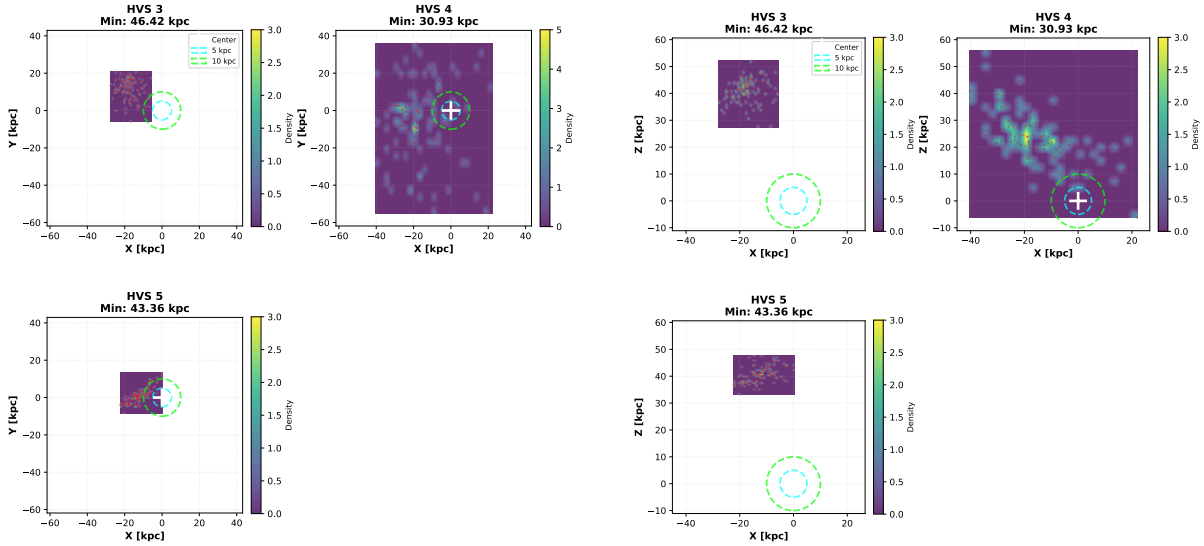

Figure 4.15: Hypervelocity satrs SMC XY and XZ closest approach.

Figure 4.15 shows Monte Carlo methodological sampled positions at closest approach to the LMC center in orthogonal projections. Distributions are broader than MW encounters,reflecting larger heliocentric distances and higherorbital uncertainties. Fewer HVS satisfy the LMC distance criterion, indicating LMC interactions are infrequent in this sample. Density maps show scattered impact parameters across both projections. Consistency between X-Y and X-Z views validates three-dimensional integration. Results suggest this sample originates primarily from the Galactic center rather than LMC ejection.

Chapter 5

Discussion

The simulations of this project reveal that the LMC and SMC follow complex, time-varying orbits within the Milky Way's gravitational potential, with sensitivity to potential model variations reaching 15–20% in orbital eccentricity. The orbital analysis identifies multiple LMC-SMC close approaches (5–20 kpc separations) occurring primarily within the past 2 Gyr, supporting first-infall models and constraining tidal mass-stripping episodes responsible for the Magellanic Stream's formation.

Most critically, the 21 hypervelocity star sample exhibits overwhelming concentration at the Galactic center (43% within 5–10 kpc), with tight Monte Carlo methodological clustering (<1.5 kpc uncertainties) validating orbital robustness. The observed characteristics—recent ejection timescales (0.07–0.25 Gyr), high velocities (237–831 km/s), and random directional distribution—match Hills mechanism predictions for supermassive black hole-driven ejection. In contrast, LMC and SMC show substantially fewer HVS approaches with broader distributions,indicating satellite-ejected HVS are rare.

Radial velocity precision emerges as the dominant observational uncertainty source, limiting orbital predictions to 6–8% accuracy for most stars. The consistency between orthogonal projections (X-Y and X-Z planes) validates our three-dimensional integration methodology. These results provide quantitative constraints on Galactic center dynamics and the efficacy of the Hills mechanism as the dominant HVS production pathway..

Chapter 6

Conclusion

This project presents an integrated computational analysis of Magellanic Cloud orbits and hypervelocity star origins within the MW+LMC+SMC system. Key findings include: (1) LMC-SMC close approaches clustered within the past 2 Gyr, constraining tidal mass-stripping timescales; (2) HVS orbital concentration at the Galactic center, with 9 of 21 stars (43%) achieving minimum distances 5–10 kpc; (3) Monte Carlo method-validated orbital uncertainties <8% for most stars, demonstrating robust predictions despite observationalmeasurement errors.

The observed HVS spatial distribution, kinematics, and directional randomness provide compelling evidence for the Hills mechanism as the dominant ejection pathway. This work demonstrates that combining modern astrometric surveys (Gaia DR3) with computational astrophysics frameworks (Galpy) and rigorous statistical methods (MCM) enables comprehensive understanding of galactic dynamics.

Limitations include potential model assumptions and the modest 21-star sample size. Future improvements through higher-resolution spectroscopy, improved Gaia astrometry, and larger HVS catalogs will refine these conclusions. This probabilistic dynamical framework provides a foundation for understanding the Magellanic System's ongoing evolution and the Milky Way's active dynamical engagement with its satellite populations. .

Bibliography

[1] C Babusiaux, C Fabricius, S Khanna, Tatiana Muraveva, C Reylé, F Spoto, Antonella Vallenari, X Luri, F Arenou, MA Alvarez, et al. Gaia data release 3-catalogue validation. *Astronomy & Astrophysics*, 674:A32, 2023.

[2] Gurtina Besla, Nitya Kallivayalil, Lars Hernquist, Roeland P van der Marel, TJ Cox, and D Kereš. Simulations of the magellanic stream in a first infall scenario. *The Astrophysical Journal Letters*, 721(2):L97, 2010.

[3] Gurtina Besla, Nitya Kallivayalil, Lars Hernquist, Roeland P van der Marel, TJ Cox, and Dušan Kereš. The role of dwarf galaxy interactions in shaping the magellanic system and implications for magellanic irregulars. *Monthly Notices of the Royal Astronomical Society*, 421(3):2109–2138, 2012.

[4] Jo Bovy. galpy: A python library for galactic dynamics. *The Astrophysical Journal Supplement Series*, 216(2):29, 2015.

[5] Subrahmanyan Chandrasekhar. Dynamical friction. i. general considerations: the coefficient of dynamical friction. *Astrophysical Journal*, 97:255–262, 1943.

[6] Gaia Collaboration, A. Vallenari, et al. Gaia data release 3. the content and survey properties. *Astronomy Astrophysics*, 674:A1, 2023.

[7] Jiwon Jesse Han, Kareem El-Badry, Scott Lucchini, Lars Hernquist, Warren Brown, Nico Garavito-Camargo, Charlie Conroy, and Re'em Sari. Hypervelocity stars trace a supermassive black hole in the large magellanic cloud. *The Astrophysical Journal*, 982(2):188, 2025.

[8] Lars Hernquist. An analytical model for spherical galaxies and bulges. *The Astrophysical Journal*, 356:359, 1990.

[9] Plotly Technologies Inc. Collaborative data science, 2015.

[10] Dean RH Johnson and David R Soderblom. Calculating galactic space velocities and their uncertainties, with an application to the ursa major group. *Astronomical Journal (ISSN 0004-6256), vol. 93, April 1987, p. 864-867.*, 93:864–867, 1987.

[11] Andrey Kravtsov and Sophia Winney. Effect of the large magellanic cloud on the kinematics of milky way satellites and virial mass estimate. *arXiv preprint arXiv:2405.06017*, 2024.

[12] Xavier Luri, L Chemin, Gisella Clementini, HE Delgado, Paul J McMillan, Manuel Romero-Gómez, E Balbinot, A Castro-Ginard, R Mor, V Ripepi, et al. Gaia early

data release 3-structure and properties of the magellanic clouds. *Astronomy & Astrophysics*, 649:A7, 2021.

[13] Paul J McMillan. The mass distribution and gravitational potential of the milky way. *Monthly Notices of the Royal Astronomical Society*, page stw2759, 2016.

[14] Francesco Montanari, David Barrado, and Juan García-Bellido. Searching for correlations in gaia dr2 unbound star trajectories. *Monthly Notices of the Royal Astronomical Society*, 490(4):5647–5657, 2019.

[15] Ben Moore and Marc Davis. The origin of the magellanic stream. *Monthly Notices of the Royal Astronomical Society*, 270(2):209–221, 1994.

[16] Erik Muller, Lister Staveley-Smith, William Zealey, and S Stanimirović. High-resolution h i observations of the western magellanic bridge. *Monthly Notices of the Royal Astronomical Society*, 339(1):105–124, 2003.

[17] Slawomir Piatek, Carlton Pryor, and Edward W Olszewski. Proper motions of the large magellanic cloud and small magellanic cloud: re-analysis of hubble space telescope data. *The Astronomical Journal*, 135(3):1024, 2008.

[18] Roeland P Van der Marel and Nitya Kallivayalil. Third-epoch magellanic cloud proper motions. ii. the large magellanic cloud rotation field in three dimensions. *The Astrophysical Journal*, 781(2):121, 2013.

[19] MC Wyatt, A Bonsor, AP Jackson, S Marino, and A Shannon. How to design a planetary system for different scattering outcomes: giant impact sweet spot, maximising exocomets, scattered disks. *Monthly Notices of the Royal Astronomical Society*, page stw2633, 2016.

Approval

The internship report titled “Calculating Orbits of the Dwarfs and High Velocity Stars of Milky Way” submitted by Upendra Sen Chakma, a participant of the ICTP PWF: Physics for Bangladesh Online Summer Internship, has been found satisfactory in partial fulfillment of the requirements of the internship program. The internship was conducted under the supervision of **Istiak Hossain Akib** during the period **15 July 2025** to **15 October 2025**.

Supervisor

Istiak Hossain Akib

Observatoire de Paris